Available online at www.sciencedirect.com
ScienceDirect
Journal of Hydrodynamics
2012,24(2):226-234
DOI: 10.1016/S1001-6058(11)60238-2

ELSEVIER

www.sciencedirect.com/
science/journal/10016058

RESEARCH OF INNER FLOW IN A DOUBLE BLADES PUMP BASED ON OPENFOAM*

LIU Hou-lin, REN Yun, WANG Kai, WU Deng-hao, RU Wei-min,TAN Ming-gao
Research Center of Fluid Machinery Engineering and Technology, Jiangsu University, Zhengjiang 212013, China,
E-mail: liuhoulin@ujs.edu.cn

(Received September 24, 2011, Revised January 9, 2012)

Abstract: The inner flow analysis of centrifugal pumps has gradually become an important issue for the hydraulic design and performance improvement. Nowadays, CFD simulation toolbox of pump inner flow mainly contains commercial tools and open source tools. There are some defects for commercial CFD software for the numerical simulation of 3-D turbulent internal flow in pump, especially in capturing the flow characteristics under the off-design operating conditions. Additionally, it is difficult for researchers to do further investigation because of the undeclared source. Therefore, an open source software like Open Field Operation and Manipulation (OpenFOAM) is increasingly popular with researchers from all over the world. In this paper, a new computational study was implemented based on the original solver and was used to directly simulate the steady-state inner flow in a double blades pump, with the specific speed is 111. In order to disclose the characteristics deeply, three research schemes were conducted. The ratios (Q/Q_d) of the flow rate are 0.8, 1.0 and 1.2, respectively. The simulation results were verified with the Particle Imaging Velocimetry (PIV) experimental results, and the numerical calculation results agree well with the experimental data. Meanwhile, the phenomena of flow separation under the off-design operating conditions are well captured by OpenFOAM. The results indicate that OpenFOAM possesses obvious strong predominance in computing the internal flow field of pump. The analysis results can also be used as the basis for the further research and the improvement of centrifugal pump.

Key words: numerical simulation, double blades pump, internal flow, Particle Imaging Velocimetry (PIV)

Introduction

Double blades pumps is a kind of centrifugal pump with two blades. There are two symmetrical curve impeller passages from its inlet to outlet and the impeller outlet is quite wide. Therefore, it usually becomes one of impeller shapes in solid-liquid two-phase centrifugal pump. However, due to the short development history and the imperfect design theory, its impellers are often designed with a combination of experience of the designers so far in practice, so that its performance and stability are not ensured[1-3]. Determining the pump performance is decided by examining its inner flow characteristics is undoubtedly the best method to improve the performance of pumps[4-6]. Recently, with the rapid progress in CFD and computer technology, the internal flow simulation has gradually become the important foundation of optimization and design for turbo-machinery[7-10]. Now, the fluid machinery CFD simulation toolbox mainly contains commercial tools and open source tools. Over the years, the commercial software packages are fashionable in the world by its abundant function and fine easy-use quality. On the other hand, as a CFD software, commercial tool is not very professional, the computational results for pumps are less than satisfactory, especially in capturing the flow characteristics under the off-design operating conditions. Furthermore, its undeclared source brings a considerable inconvenience for the application of numerical simulation in fluid machineries. Although codes can be added to implementation through user-define-functions, it has a strong limitation. For example, when the SIMPLE algorithm and two-equation turbulence

* Project supported by the National Natural Science Funds for Distinguished Young Scholar (Grant No. 50825902), the National Natural Science Foundation of China (Grant Nos. 51079062, 51179075 and 51109095) and the Natural Science Foundation of Jiangsu Province (Grant Nos. BK2009006, BK2010346).

Biography: LIU Hou-lin (1971-), Male, Ph. D., Professor

© 1994-2013 China Academic Journal Electronic Publishing House. All rights reserved. http://www.cnki.net

models have to be improved, one need to have a through understanding of the governing equations, discretization method, turbulence models and iteration algorithm. However, the core algorithm code and data processing method can not be acquired because of commercialization and only several options can be chosen. Therefore, many open source CFD software are becoming popular and a high quality open source CFD simulation platform like the Open Field Operation and Manipulation (OpenFOAM) is outstanding due to its powerful function, clear architecture, expand feature and unified format.

The OpenFOAM CFD toolbox was released as an open source December 10, 2004, which is based on C++ routine and contains many C++ modules which can be freely combined with some other modules such as tensor, vector, turbulence models, numerical algorithm, discretion modules, automatic control modules and so on. Therefore, it is convenient to employ its solvers in simulating complex physical models in chemical reaction, turbulent flow and heat conduction, etc..

A variety of work on the internal flow in fluid machinery via OpenFOAM was done. Nilsson[11] conducted the steady and unsteady computation of the flow in the Hǒllerforsen turbine runner and draft tube, and compared the results obtained by the OpenFOAM with those by the CFX-5 and in experiments. Eventually, the applicability and reliability of the OpenFOAM in a Kaplan water turbine runner and draft tube was verified. Petit et al.[12] validated an implementation of the General Grid Interface (GGI) in the OpenFOAM by using the frozen rotor steady approach and the sliding grid unsteady approach. However, all the simulations were performed for a simplified 2-D model of a centrifugal pump. Li[13] simulated boundary layer in wind tunnel by OpenFOAM, which revealed that it was suitable for using OpenFOAM to conduct a Computational Wind Engineering (CWE) research. Currently, there is not much work regarding the study of the inner flow of pumps through comparison between the OpenFOAM simulation and experiments, and the related reports are seldom found.

As an open source code, the OpenFOAM provides direct access to models and solver implementation details. However, there are some defects for the OpenFOAM in the numerical simulation of 3-D turbulent internal flow in hydroturbines. For the CFD simulation of hydroturbines, separate 3-D mesh passages or full geometry are generally connected together in order to simulate the flow of water through a succession of complex geometries like pumps where the stationary suction and volute are located, along with the rotating impeller. The requirement to fit all the meshes with conformal matching interfaces is often very difficult or leads to geometric compromises that would affect the numerical quality of the simulation results. Therefore, there is a need for a treatment of rotor-stator interfaces, which is necessary for the simulation of the whole hydroturbines inner flow. Although the capability has existed in the OpenFOAM, there is no definition in the case directory. There is also a need for a set of boundary conditions that makes it easy to capture basic features in a similar way as it can be done in some other CFD solvers. Furthermore, relaxation factors which control under-relaxation, have an important influence on improving stability of a computation. However, there is no guiding principle about those factors. Therefore, the paper focuses on centrifugal pump with the consideration of these factors. The numerical simulation of pump by using the OpenFOAM is achieved and the computational results are verified by Particle Imaging Velocimetry (PIV) experiments. The research also provides the foundation for achieving higher computation accuracy of pump inner flow by improving the CFD method with self-compiling program in the OpenFOAM.

In this paper, in order to compute the interactions between rotating and fixed components in pumps, a Multiple Reference Frames (MRF) solver is used. At the same time, the simulation results are also validated by PIV test. The operating system used is SUSE Linux 10.3, and the version number used for the present computations is OpenFOAM 1.5-dev.

1. Numerical method and model

1.1 *Governing equations*

The OpenFOAM toolbox already provides a solver called MRFSimpleFoam for solving the steady-state Reynolds-Averaged Navier-Stokes equations with turbulence models, such as the standard $k-\varepsilon$ model. The coupling between velocity and pressure is treated using the SIMPLE method[14]. The MRFSimpleFoam solver employs the finite-volume technique to discretize the Navier-Stokes equations in the rotating reference frame:

$$\nabla \cdot \boldsymbol{u}_R = 0$$

$$\nabla \cdot (\boldsymbol{u}_R \otimes \boldsymbol{u}_R) + 2\boldsymbol{\Omega} \times \boldsymbol{u}_R + \boldsymbol{\Omega} \times \boldsymbol{\Omega} \times \boldsymbol{r} = -\nabla\left(\frac{p}{\rho}\right) + \nu \nabla \cdot \nabla \boldsymbol{u}_R$$

where $\boldsymbol{u}_R$ is flow velocity in rotating frame, $\boldsymbol{\Omega}$ rotating frame speed, $\boldsymbol{r}$ position vector, p fluid pressure, ρ fluid density, and ν the kinematic viscosity.

1.2 *General Grid Interface (GGI)*

Due to the interaction between stator and rotor,

© 1994-2013 China Academic Journal Electronic Publishing House. All rights reserved. http://www.cnki.net

how to cope with the grids and information transmission of the coupling parts in the computational domain is a key issue to simulate precisely the flow fields[15-17]. The frozen rotor method in MRFSimpleFOAM solver is a steady-state formulation where the relative positions in rotor and stator are fixed. In the same time frame, the rotor and the stator parts will be meshed separately. For non-stationary turbo-machinery simulations, the relative rotation of mesh parts will necessarily produce non-conformal interfaces between the fixed and moving sections. A connection between these meshes is needed in order to simplify the mesh complexity in various turbo-machinery simulations and hence reduce the computer time cost. The GGI, developed by Beaudoin and Jasak[18] can be used for that purpose in OpenFOAM. It is a new coupling interface for OpenFOAM, joining multiple non-conformal regions where the patches nodes on each side of the interface do not match.

This interface uses weighted interpolation to evaluate and transmit flow values across a pair of conformal or non-conformal coupled patches. The basic GGI interface is similar to a case of "static" sliding interfaces with the advantage that no remeshing is required for the neighboring cells of the interface.

The GGI uses the Sutherland-Hodgman algorithm[12] for computing the master and shadow face intersection area. Some quick rejection algorithms based on an axis aligned bounding box have been implemented to speed up the search for potential face neighbors. Then, in order to rapidly handle the final non-overlapping filtering test, an efficient Hormann-Agathos point-in-polygon algorithm[19] has been included into the separating axis theorem algorithm[18]. Finally, discretization effects are taken into account in order to properly scale the GGI weighting factors to handle the possible presence of non-overlapping faces and hence keep the GGI interface conservative.

1.3 *Boundary and initial conditions*

While the Partial Differential Equation (PDE) is solved with the finite volume method, a suitable interpolation scheme of values typically from cell centres to face centres has a great effect on the numerical results, especially for the convection term. The convection scheme of the existing solver is specified as default by limited linear differencing, which is a Total Variation Diminishing (TVD) scheme. Although it offers a second-order accurate discretization scheme for the convection term, it creates an unconditionally unstable discretisation practice[20]. In order to achieve stability, a fist-order accurate upwind differencing scheme has been introduced and the simulation results show that the TVD scheme can result more easily in iteration divergence and computation failure than the upwind differencing scheme in simulating the pump inner flow. Therefore, TVD scheme is not applicable to simulate the pump inner flow in the OpenFOAM. In this paper, Guassian up-wind scheme is used and can get the satisfactory results in numerical tests.

In addition to appropriate discretization schemes, under-relaxation is another important technique used for improving the stability of a computation, particularly in solving steady-state problems. Under-relaxation works by limiting the amount, in which a variable changes from one iteration to the next, either by limiting the solution matrix and source prior to solving for a field or by modifying the field directly. An under-relaxation factor α, $0<\alpha\leqslant 1$ specifies the amount of under-relaxation, ranging from none at all for $\alpha=1$ and increasing in strength as $\alpha\to 0$. Therefore, selecting an appropriate relaxation factor has great influence on the efficiency of computation. If the relaxation factor is too large, it will lead to divergence of computation easily. If it is too small, the result will converge slowly. Besides, an appropriate relaxation factor depends on the specific problem itself. Thus, there is no instruction about relaxation factor in simulating pump inner flow. At the same time, if the relaxation factors are used by default in the OpenFOAM to examine the pump inner flow, the result will be unstable. In this paper, the relaxation factors are suitable for simulating the pump inner flow according to $\alpha_u+\alpha_p=1$ [20]. At last, the relaxation factors are determined after many tests and the under-relaxation factors of relevant variables (i.e., pressure, momentum, turbulence kinetic energy and turbulence dissipation rate) are 0.3, 0.7, 0.3 and 0.3, respectively.

In order to simulate the flow field in and the whole pump, the GGI method is needed to transmit the information between rotor and stator.

1.4 *Model*

A 3-D model of double-blade pump for simulation is generated by Pro/E. The suction chamber is designed by semi-spiral method, while the volute is designed by equal velocity moment method and the cross section is rectangular, and type line is the logarithmic spiral. The design parameters of the double blades pump are shown in Table 1.

Herein the calculation formulas of n_s is

$$n_s=\frac{3.65n\sqrt{Q}}{H^{3/4}}$$

Before the simulation, studying the grid independency and selecting the turbulent model are necessary[21,22]. The geometry is meshed in hybrid grid by GAMBIT and the OpenFOAM is used to simulate the inner flow in the double-blade pump. The data for studying grid independency are shown in Table 2. If the head difference is smaller than 0.2%, the grid number is acceptable. According to the computation, Scheme 2 meets the need. So Scheme 2 of grid is adopted. The grids are show in Fig.1.

© 1994-2013 China Academic Journal Electronic Publishing House. All rights reserved. http://www.cnki.net

Table 1 The design parameters

Parameter	Sign	Value
Flow rate	Q (m^3/h)	25.86
Head	H (m)	2.53
Rotation speed	n (r/min)	750
Specific speed	n_s	111
Suction chamber inlet diameter	D_s (m)	0.08
Impeller inlet diameter	D_i (m)	0.09
Blade inlet diameter	D_1 (m)	0.0812
Impeller outlet diameter	D_2 (m)	0.2
Impeller outlet width	b_2 (m)	0.047
Blade inlet angle	β_1 (^{o})	18.3
Blade outlet angle	β_2 (^{o})	30
Volute base circle diameter	D_3 (m)	0.212
Volute inlet width	b_3 (m)	0.077

Table 2 Data for studying grid independency

No.	Grid number				Head, H (m)
	Impeller	Volute	Suction	Total	
1	618 738	220 175	300 103	1 139 016	2.46034
2	577 913	179 340	255 937	1 013 190	2.45974
3	505 999	143 450	202 830	852 279	2.43180
4	378 565	151 341	99 619	629 525	2.40151

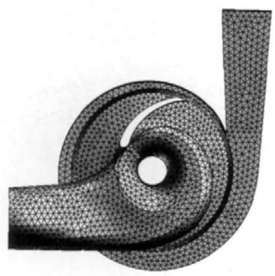

Fig.1 Grids

Table 3 Comparison of turbulence models

Turbulent model	Head, H (m)
Standard $k-\varepsilon$	2.45974
RNG $k-\varepsilon$	2.44706
Omega SST	2.42225

The standard $k-\varepsilon$, RNG $k-\varepsilon$ and Omega SST turbulence models have been used to simulate the inner flow in centrifugal pumps. With the same grid, the comparison among the three turbulence models was made and the results are shown in Table 3. It is found that compared with the experimental data, the head obtained by standard $k-\varepsilon$ model is the most accurate. Therefore, the standard $k-\varepsilon$ turbulence model is used to perform the simulation in this paper.

For the test region, the impeller passage near the volute tongue is selected. In order to analyze the inner flow better, 7 pieces of plane curve are set in the impeller mid-height, equidistant from the impeller inlet to the impeller outlet, and 12 points are distributed equidistantly on each curve. All the analyses of post processing in this paper are based on those monitoring points as shown in Fig.2.

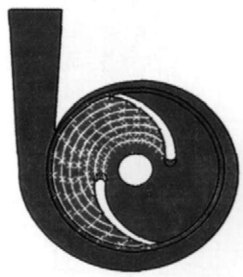

Fig.2 Sample points

In order to disclose the characteristics effectively, three research schemes are presented. The ratios (Q/Q_d) of the flow rate are 0.8, 1.0 and 1.2, respectively.

2. Results and analysis

2.1 *Relative velocity distribution*

The relative velocity distributions are illustrated in Fig.3. It can be seen that from inlet to outlet under the same working condition, there is a low-speed zone near the middle of the pressure side at the inlet, along the direction of speed changed, which can be found in the top view of Fig.3. Then, a back flow vortex appears, with a remarkable jet-wake flow model. Furthermore, the velocities of all points in the low speed zone go upward with the increase of radius and the jet-wake flow feature becomes unnoticeable, finally disappears. On the circle of impeller inlet, the relative velocities decline gradually at first, from the suction side nearby to the pressure side nearby, and then, when it comes close to the pressure side, the velocity goes up again, peaking at the pressure side. With the increase of radius, the variations of velocity near the suction side are less regular than that near the pressure side. However, when starting from the middle of impeller passage, the velocity near the suction side rises gradually with the increase of radius. But the velocity near the pressure side always rise with the increase of radius. Moreover, the velocity gradient near the pressure side is larger than that near

© 1994-2013 China Academic Journal Electronic Publishing House. All rights reserved. http://www.cnki.net

the suction side. On the outlet circle, the velocity goes up gradually from the suction side. The flow in impeller passages is asymmetric due to the effect of volute. Particularly, the relative velocity of points near the volute tongue rise fastest, peaking at the patch slightly below the volute tongue. After that, they decline. In short, the values of velocity of points near the volute tongue are greater than that far from the tongue.

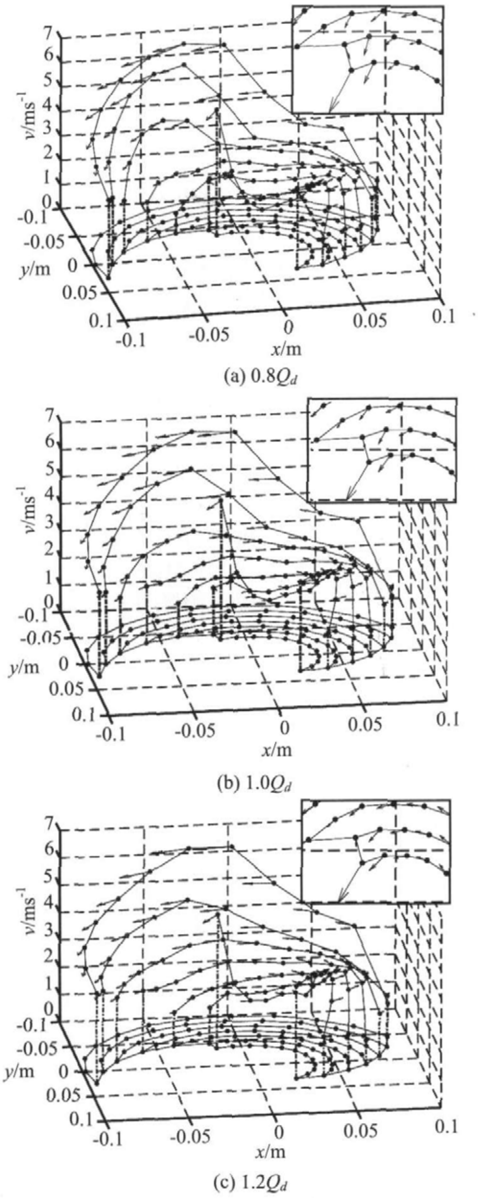

Fig.3 relative velocity distribution in impeller passage and its local top view

Under the same working condition, at the edge of the passage on the inlet circle, the velocity near the pressure side is much greater than that near the suction side. Besides, on the same circle near the inlet, the velocity near the suction side are greater than that near the pressure side. With the increase of radius, the gaps between the pressure side and suction side are narrowing and the velocities on those two sides tend to equal at the middle passage, and thus an equal speed area is formed. Then, the velocity near the pressure side is far greater than that near the suction side.

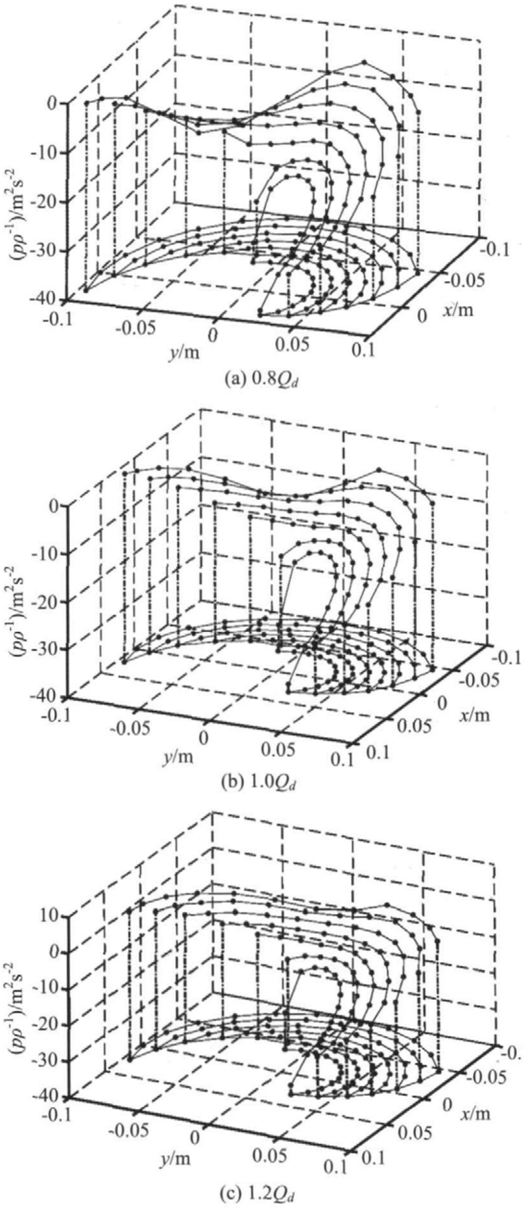

Fig.4 Static pressure distribution in impeller passage

Under different working conditions, the jet-wake model at the same position still holds. But with the increase of flow, the velocity of points in the backward flow vortex area also increase, while the scope reduces, and the feature with jet-wake model becomes less and less significant. The whole passage with the low flow conditions, the velocity reaches its minimum at the middle of the pressure side near the inlet, while peaking at the patch slightly below the volute tongue. Meanwhile, with the increase of flow, the greatest velocity in the whole passage decreases, the equal speed area enlarges, and gradually approaches impeller outlet.

© 1994-2013 China Academic Journal Electronic Publishing House. All rights reserved. http://www.cnki.net

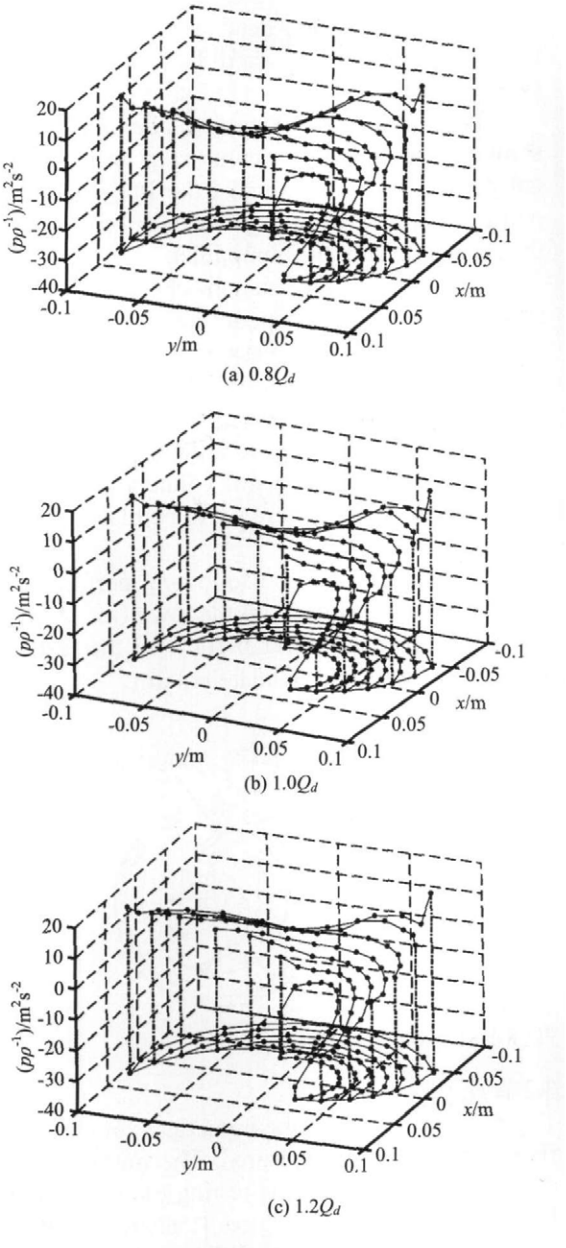

Fig.5 Total pressure distribution in impeller passage

2.2 *Static pressure and total pressure distribution*

The static pressure distribution and total pressure distribution of each point under different working conditions are illustrated in Fig.4 and Fig.5 respectively. It can be seen from Fig.4 that under the same working condition, the static pressures, at inlet patch near the pressure side, have a larger fluctuation than at other points of the same circle and are more irregular. Static pressure increases as the radius increases, except for that at outlet circle. The static pressure, at outlet circle and near the volute tongue, experiences a considerate reduction and the values are clearly lower than those nearby. Furthermore, the values of static pressure near the inlet rise and then gradually decline from the pressure side to the suction side. With the increase of radius, the values of static pressure near the pressure side increases suddenly, resulting in the static pressure variation near the pressure side are less regular than that near the suction side. In all, the static pressure near pressure side is much higher than that near the suction side at the same radius.

The static pressure near the pressure side is higher than that near the suction side near the inlet circle. Starting from the middle circle of impeller passage, the static pressure near the suction side is higher than that near the pressure side. It can be seen from the whole distribution of static pressure on impeller passage, the lowest static pressure is near the suction side of impeller inlet, an the reason may be that the eddy is generated near the suction side due to the flow inside the impeller is impacted by the leading edge of blade. The highest static pressure is near the pressure side of outlet, which illustrates that the flow inside the impeller is influenced not only by the structure of impeller, but also by the volute indeed. With the increase of flow, static pressure at each point increases dramatically, however, the static pressure distribution between the pressure side and suction side does not go up with same drastic speed. In fact, static pressure near the pressure side increases a little faster than that near the suction side. Meanwhile, the static pressure near the volute tongue becomes unnoticeable and at several points the same static pressure appears at the middle passage under the high flow condition. Moreover, the area with equal static pressure extends to the suction side as the flow is higher.

From the Fig.5, it can be seen that the features of total pressure distribution are similar with that of static pressure. However, under the low flow conditions, the corresponding total pressure of each circle does not always goes up as the radius increases. Instead, when the circle come close to impeller outlet, the total pressure near the middle patch of the suction side falls rapidly as the radius increases. In addition, points with this feature tend to expand to the pressure side. However, the feature becomes obscure under the high flow condition. From the whole impeller passage, the total pressure still reaches its minimum on the suction side of impeller inlet, while peaking at the suction side of impeller outlet. Naturally, near the outlet of impeller, there are high and low total pressure zone due to the influence of wake flow. Specifically, the low total pressure zone is located at the passage of the volute tongue nearby while the high total pressure zone is near the pressure side, and they are very obvious under the low flow conditions. But, under the high flow conditions, the total pressure goes up again, except at the point near the volute tongue, where a sharp fluctuation appears.

© 1994-2013 China Academic Journal Electronic Publishing House. All rights reserved. http://www.cnki.net

3. PIV test

3.1 *Experimental facilities*

The PIV system applied in this experiment is a 3-D PIV system of TSI Inc. produced in 2009. It mainly includes the following five equipments. The first is U.S. New Wave's YAG200-NWL pulse laser, whose single pulse energy is 200 mJ, laser pulse frequency is 30 Hz, duration is 3 ns-5 ns, and beam diameter is 0.0035 m. The second is the 610 035 laser pulse synchronizer, whose trigger timing accuracy is up to 1 ns. The third is the 630 059 powerview plus 4M PIV camera, which is the lightest CCD camera in similar products, with 2 048×2 048 light sensitive pixels and 16 frames/second frame rate. The fourth is the insight 3G software, which is used in data acquisition, analysis, and displays software platform, embedded "Hart" correlation algorithm engine and Tecplot flow field analysis software. The fifth is the 610 015 light arm and light source lens, etc..

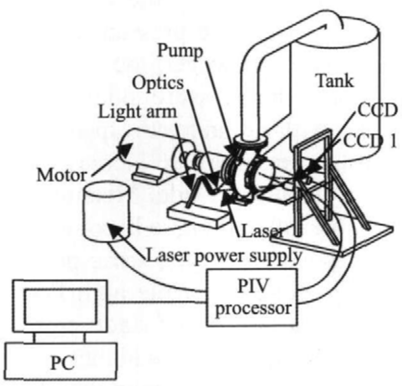

Fig.6 Sketch of experiment set-up

The Fig.6 shows the sketch of the experiment rig. All the experiments were complected in Jiangsu University. The experiments were conducted in an open loop, which consists of a tank open to air, a suction valve, a test pump, a discharge pipe and a discharge valve. The model pump has a single axial suction and a volute casing. In the circuit, water was pumped from and returned to a huge reservoir. The flow rate was regulated by the discharge valve and was measured by electromagnetic flow meter. The rotation speed was detected by plus signals.

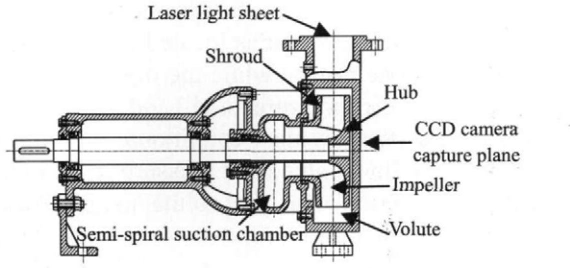

Fig.7 Structure of double-blade model pump

Flow rate uncertainties are found to be always smaller than 0.5%. The head and efficiency uncertainties are kept under 1% and 1.5%, respectively. The experiment data are shown in Table 1.

The structure of double-blade model pump is shown in Fig.7. It is different from ordinary centrifugal pumps. In order to make the PIV test easily, the pump shaft, passing through the suction chamber, is at the same side with the pump inlet.

The semi-spiral suction chamber is made of stainless steel, while impeller and volute are made of organic glass. Organic glass is homogeneous, bubble-free and smooth. Meantime all surfaces of organic glass are polished, with the roughness is up to 3.2.

In addition, in order to reduce background noise, there is no tested surfaces of volute and impeller near to the suction chamber are set to be black before assembly.

Finally, due to good following performance and optical property, along with the low price, Al_2O_3 powders are chosen as tracer particle in the test, and its grain diameter is approximately 8 μm.

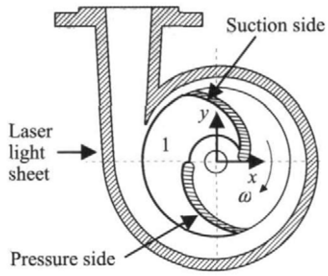

Fig.8 Testing plane and area

3.2 *Test method*

Corresponding to the numerical simulation, three flow conditions are measured. The middle section of the impeller is selected as testing plane, as shown in Fig.8. Testing area is Region 1. Shaft encoder sends out a pulse signal per revolution, which triggers the TSI synchronizer via the external trigger sync system, so that each image captured by CCD cameras is in Region 1.

3.3 *Data acquisition and processing*

Firstly, related parameters are set in the Insight 3-G software, and the sequence capture mode is used to collect 20 correlation images in each condition. Secondly, 20 images in different conditions are processed by the cross-correlation technique, and amended by techniques such as standard deviation, local mean smoothing median test and secondary peak. Then, the average of the 20 vector files are computed in Tecplot software. Finally, due to the 3-D velocity obtained in PIV tests is the absolute velocity, it is necessary to be synthesized to get the relative velocity. According to the velocity triangle method, the PIV velocity synthesis program is compiled in visual C++ 2005. More-

© 1994-2013 China Academic Journal Electronic Publishing House. All rights reserved. http://www.cnki.net

over, these vector files are also processed in Tecplot software, also.

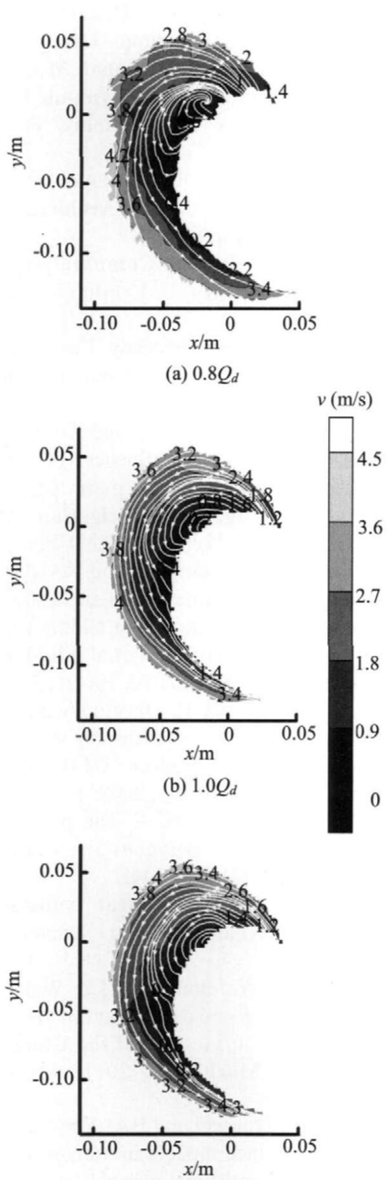

Fig.9 Contour distribution of relative velocity in PIV tests

3.4 *Test result and analysis*

The relative velocity distribution determined in the PIV measurements in the Region 1 is given in Fig.9. It can be seen that the fluid basically flows through the suction side near the impeller inlet under the same working condition. In addition, the velocity gradually increases from the impeller inlet to the impeller outlet. At the same time, a back flow vortex exists in the middle part of pressure side, with noticeable jet-wake flow feature.

In view of the three different working conditions, as the flow is higher, the gradients of relative velocities are greater while the jet-wake flow becomes less noticeable. At the same time scale, the range of the low-speed region minimized and the flow smoothed with the increase of flow. Besides, the values of relative velocity of points near the volute tongue are greater than that far from the tongue. To sum up, the test results are comparable to computational results.

4. Conclusions

New capabilities have been added to the OpenFOAM toolbox to perform steady-state MRF simulations for double-blade pump, including coupling interfaces (GGI) and specialized boundary conditions, such as discretization scheme (Guassian upwind) and under-relaxation factors. Simulations results have shown that the main characteristics of the flow fields in impeller passage of double-blade pump are well predicted. Meanwhile, the flow in impeller of the double-blade pump is tested by the PIV technique. Through comparing the results of numerical simulation and the tests results, some conclusions have been reached as follows:

Firstly, in terms of relative velocity, there is a remarkable jet-wake flow pattern near the middle of the pressure side at the inlet. As the flow rate increases, the back flow tend to disappear and the values of velocity increases gradually. Besides, the values of velocity near the volute tongue experiences serious fluctuations. In addition, under the same working condition, an equal speed area is formed at the middle passage due to the great change of velocity between the pressure side and the suction side.

Secondly, the static pressures of each circle goes up as the radius increases under the same working condition except near the volute tongue, with a considerable reduction due to the effect of volute. The feature becomes unnoticeable as the flow increases. From the whole impeller passage, the lowest static pressure appears near the suction side of impeller inlet while the highest static pressure is reached near the pressure side of outlet. Further more, there is an equal static pressure area at the middle passage under the high flow conditions, and the area expands to suction side as the flow rises.

Thirdly, the features of total pressure distribution are similar with those of static pressure. However, high and low total pressure zones exist near the outlet of impeller due to the effect of wake flow, and they are very obvious under the low flow conditions. But, under the high flow conditions, they are undistinguishable. Meanwhile, the point near the volute tongue witnesses a sharp fluctuation.

Finally, the PIV test results have a good agreement with the numerical simulation results. It indicates that the OpenFOAM is a powerful simulation platform that can add the required capabilities to better simulate complex flow behavior. It also lays the foundation of promoting the numerical accuracy and effi-

© 1994-2013 China Academic Journal Electronic Publishing House. All rights reserved. http://www.cnki.net

ciency of pump inner flow simulation by improving the algorithm and turbulence model in OpenFOAM.

References

[1] LIU J. H., ZHU M. Y. Numeration simulation of solid-liquid two-phase flow in centrifugal sewerage pump[J]. **Applied Mechanics and Materials,** 2011, 44-47: 345-348.

[2] CHEN H. L., WANG Y. and SHI G. P. Flow numerical simulation in the impeller of sewage pump[C]. **International conference on electronic and Mechanical Engineering and Information Technology.** Harbin, 2011, 3217-3220.

[3] SHAN Lin-ting. Double-channel sewage pump flow analysis and design method of the research[D]. Master Thesis, Lanzhou: Lanzhou University of Technology, 2010(in Chinese).

[4] FAN Hui-min, HONG Fang-wen and ZHANG Guo-ping et al. Applications of CFD technique in the design and flow analysis of implantable axial flow blood pump[J]. **Journal of Hydrodynamics,** 2010, 22(4): 518-525.

[5] ATIF A., BENMANSOUR S. and BOIS G. et al. Numerical and experimental comparison of the vaned diffuser interaction inside the impeller velocity field of a centrifugal pump[J]. **Science China Technological Sciences,** 2011, 54(2): 286-294.

[6] QU Li-xia, WANG Fu-jun and CONG Guo-hui et al. Effect of volute tongue-impeller gaps on the unsteady flow in double-suction centrifugal pump[J]. **Transactions of the Chinese Society for Agricultural Machinery,** 2011, 42(7): 50-55, 74(in Chinese).

[7] ZHOU Ling, SHI Wei-dong. and LU Wei-gang. Performance analysis on deep-well centrifugal pump guide vanes based on numerical simulation[J]. **Transactions of the CSAE,** 2011, 27(9): 38-42(in Chinese).

[8] WESTRA R. W., BROERSMA L. and Van ANDEL K. et al. PIV measurements and CFD computations of secondary flow in a centrifugal pump impeller[J]. **Journal of Fluids Engineering**, 2010, 132(2): 061104.

[9] ZHANG De-sheng, SHI Wei-dong and CHEN Bin et al. Unsteady flow analysis and experimental investigation of axial-flow pump[J]. **Journal of Hydrodynamics,** 2010, 22(1): 35-43.

[10] CHANG Shu-ping, WANG Yong-sheng. Optimal design of impeller for residual heat removal pumps based on numerical simulation of 3D turbulent flow[J]. **Journal of Drainage and Irrigation Machinery Engineering,** 2011, 29(5): 397-400(in Chinese).

[11] NILSSON H. Evaluation of OpenFOAM for CFD of turbulent flow in water turbines[C]. **23rd IAHR Symposium on Hydraulic Machinery and Systems.** Yokohama, Japan, 2006.

[12] PETIT O., PAGE M. and BEAUDOIN M. et al. The ERCOFTAC centrifugal pump OpenFOAM case-study[C]. **3rd IAHR International Meeting of the Workgroup on Cavitation and Dynamic Problems in Hydraulic Machinery and Systems.** Brno, Czech, 2009.

[13] LI Sun-wei. Simulating boundary layer in wind tunnel using OpenFOAM[J]. **Shanxi Architecture**, 2008, 34(23): 70-71(in Chinese).

[14] FERZIGER J. H., PERIC M. **Computational methods for fluid dynamics**[M]. 3rd Edition, New York: Springer-Verlag, 2002.

[15] JOSÉ G., CARLOS S. Unsteady flow structure and global variables in a centrifugal pump[J]. **Journal of Fluids Engineering,** 2006, 128(5): 937-946.

[16] GUO Peng-cheng, LUO Xing-qi and ZHOU Peng et al. Numerical simulation of influence of volute with different sections on centrifugal pump performance[J]. **Journal of Drainage and Irrigation Machinery Engineering,** 2010, 28(4): 300-304(in Chinese).

[17] HUANG S., MOHAMAD A. A. and NANDAKUMAR K. et al. Numerical simulation of unsteady flow in a multistage centrifugal pump using sliding mesh technique[J]. **Progress in Computational Fluid Dynamics, An International Journal,** 2010, 10(4): 239-245.

[18] BEAUDOIN M., JASAK H. Development of a generalized grid interface for turbomachinery simulations with OpenFOAM[C]. **Open Source CFD International Conference.** Berlin, Germany, 2008, 1-11.

[19] HORMANN K., AGATHOS A. The point in polygon problem for arbitrary polygons[J]. **Computational Geometry,** 2001, 20(3): 131-144.

[20] TAO Wen-quan. **Numerical heat transfer**[M]. 2nd Edition, Xi'an: Xi'an Jiaotong University Press, 2001(in Chinese).

[21] ZHOU Ling, SHI Wei-dong and LU Wei-gang et al. Numerical simulation and experiment on deep-well centrifugal pump[J]. **Transactions of the Chinese Society for Agricultural Machinery,** 2011, 42(3): 69-73(in Chinese).

[22] LIU Mei-qing, LI Qiu-wei and BAI Yao-hua et al. Applicability of turbulence models in numerical simulation of double suction centrifugal pump[J]. **Transactions of the Chinese Society for Agricultural Machinery,** 2010, 41(Suppl.): 6-9, 26(in Chinese).

© 1994-2013 China Academic Journal Electronic Publishing House. All rights reserved. http://www.cnki.net